# Freezing lines of colloidal Yukawa spheres.

# I: A Rogers-Young integral equation study

**Jacek Gapinski[*1], Gerhard Nägele[2], and Adam Patkowski[1]**

[1] *Faculty of Physics, A. Mickiewicz University, Umultowska 85, 61-614 Poznań, Poland*
[2] *Institute of Complex Systems (ICS-3), Forschungszentrum Jülich, D-52425 Jülich, Germany*

**Abstract**

Using the Rogers-Young (RY) integral equation scheme for the static structure factor combined with the one-phase Hansen-Verlet (HV) freezing rule, we study the equilibrium structure and two-parameter freezing lines of colloidal particles with Yukawa-type pair interactions representing charge-stabilized silica spheres suspended in dimethylformamide (DMF). Results are presented for a vast range of concentrations, salinities and effective charges covering particles with masked excluded-volume interactions. The freezing lines were obtained for the low-charge and high-charge solutions of the static structure factor, for various two-parameter sets of experimentally accessible system parameters. All RY-HV based freezing lines can be mapped on a universal fluid-solid coexistence line in good agreement with computer simulation predictions. The RY-HV calculations extend the freezing lines obtained in earlier simulations to a broader parameter range. The experimentally observed fluid-bcc-fluid reentrant transition of charged silica spheres in DMF can be explained using the freezing lines obtained in this work.

[*] gapinski@amu.edu.pl

globular proteins in water such as apoferritin [12-13] or bovine serum albumin (BSA) [14-15].

The pair potential in Eq. (1) depends on four dimensionless parameter groups $\{L_B/\sigma, Z, C_s\sigma^3, \phi\}$, which can be controlled experimentally to a larger extent. However, the important subclass of systems with masked hard-core interactions is completely characterized by two independent parameters only [16]. A convenient choice of these parameters for theoretical discussions is [16]

$$\lambda = \kappa\langle r\rangle \tag{3}$$

$$\tilde{T} = \frac{k_B T}{u(\langle r\rangle)} \tag{4}$$

where $\lambda$ is the geometric (simple-cubic) mean particle distance, $\langle r\rangle = n^{-1/3}$, expressed in units of the Debye screening length $\kappa^{-1}$, and $\tilde{T}$ measures the thermal energy relative to the potential energy, $u(\langle r\rangle)$, of a pair of particles at distance $r = \langle r\rangle$. Different combinations of the four parameters $\{L_B/\sigma, Z, C_s\sigma^3, \phi\}$ sharing the same fluid-phase state point $\{\lambda, \tilde{T}\}$ also share the same static structure factors, $S(q)$, and radial distribution functions (rdf), $g(r)$, for the scattering wavenumber $q$ and pair distance $r$ measured in units of $\langle r\rangle$ [17-18].

The universal $\lambda - \tilde{T}$ phase diagram of these effectively point-like Yukawa particles is quite simple, and has been well explored over the past twenty years [16-17,19-27]. It consists of a single (supercritical) fluid phase that can freeze into an fcc or a bcc solid, characterized by eight or twelve next neighbor particles, respectively. The phase diagram has a single triple point but no critical point, since the pair interactions in this one-component system are purely repulsive.

Note that the extended phase diagram not considered in the present work, where the $g(r)$ of hard-sphere-Yukawa particles is allowed to be discontinuous at contact distance,

freezing becomes increasingly unstable against spontaneous density modulations of wave vectors of magnitude near $q_m$ which at freezing change the uniform fluid density profile to the periodic profile of the crystal [29-30].

The RY-HV method allows for a conveniently fast, and as we will show in comparison to the universal $\tilde{T}$ - $\lambda$ diagram, quite accurate calculation of freezing lines in various parameter representations. A detailed study of experimental-parameter freezing lines on the basis of computer simulations or elaborate density functional theory calculations of similar generality as the one presented here, would have been numerically very expensive and time consuming. We show that the fast RY-HV method predicts a universal freezing line in the $\lambda - \tilde{T}$ phase-space in good overall agreement with simulation results by Stevens and Robbins [22], Meijer and Frenkel [20] and Hamaguchi *et al.* [23], however extending these earlier results to substantially larger values of $\lambda$. Note here again that, while $\lambda - \tilde{T}$ phase space considerations are important from a theoretical viewpoint, the experimentally controllable parameters such as salt concentration and effective charge cannot be uniquely determined from $\lambda$ and $\tilde{T}$ alone. The good agreement justifies our usage of the RY-HV scheme in studying various structural properties under freezing conditions. As an interesting experimental result, we will show that the most recent and most accurate Yukawa spheres simulation result by Hamaguchi *et al.* [23] for the bcc - fcc coexistence line, which is located in $\tilde{T}$ - $\lambda$ phase space noticeably away from the one predicted by Robbins *et al.* [16], and for the bcc phase region extending to $\lambda$ values substantially larger than the one in [16], is fully consistent with our X-ray scattering data for silica spheres in DMF.

For neutral hard spheres, one finds $S_f(q_m) = 2.85$ at freezing [31]. For the charge-stabilized colloidal systems with soft Yukawa repulsion studied in this work, where the hard core plays no physical role, a constant value of $S_f(q_m) = 3.1$ is used. This value is in

applications. To gain a complete survey on two-parameter freezing lines, both the low-charge branch and high-charge branch solutions for $S(q)$ have been determined and discussed, on pointing to differing trends which allow for distinguishing these solutions. Our discussion should prove helpful in deciding which of the two solutions (i.e., which of the two in general largely different effective charge numbers) is the physical one for the system under study.

The present paper is not concerned with the on-going discussion on how the effective charge, $Ze$, in Eq. (1) is quantitatively related to a bare particle charge, commonly referred to as the colloid charge renormalization problem. The bare charge is usually defined on a more fundamental, so-called Primitive Model level of description where the colloidal particle and the microions are treated equally as uniformly charged spheres of different sizes. Poisson-Boltzmann type cell model [33], renormalized jellium model methods [34-36], and non-mean-field generalizations accounting for the effect of multivalent microions [37], have been derived which allow for calculating the effective charge approximately as a function of volume fraction, salt concentration, and bare colloid charge. Noteworthy here is a recent phase diagram calculation [36] for Yukawa spheres with built-in (approximate) charge renormalization, for particles at constant zeta potential. We refrain here from including charge-renormalization into our quantitative analysis of freezing lines, not only for maintaining the paper in an acceptable size, but also since the calculated renormalized charge values can differ substantially, depending on the charge renormalization method and the invoked chemical charge regulation scheme.

We are also not dealing here with the exploration of non-pairwise additivity effects in the electrostatic interactions which can play a role for $\lambda \leq 2$, i.e. for deionized suspensions of comparatively large particle concentrations [17].

The present paper (labeled I) focuses on the construction and discussion of freezing lines in terms of experimentally accessible parameters. In a related forthcoming paper by the

role, a constant peak height value of $S_f(q_m) = 3.1$ is used to characterize the onset of freezing into a crystalline state. The employed RY method is a hybrid method which interpolates continuously between the Percus-Yevick closure at small, and the hypernetted chain closure at long distances, by a single-parameter mixing function. The mixing parameter is determined by imposing local thermodynamic consistency, i.e., by enforcing equality between the isothermal compressibilities derived from the compressibility and virial (pressure) equation of states. For details see [38]. The RY method has been found, from numerous comparisons with simulation results for $S(q)$ and $g(r)$ (see, e.g., [18,39]), to perform excellently for the (three-dimensional) hard-sphere plus repulsive Yukawa pair potential. Note that in this work we use the RY method solely to calculate the pair correlation functions, not addressing the thermodynamic subtleties which one faces for systems with state-dependent pair potentials.

The system parameters employed in the theoretical calculations represent suspensions of monodisperse silica spheres of diameter $\sigma = 2a = 171$ nm and mass density $\rho = 1.95$ g/cm$^3$ in DMF ($\varepsilon = 36.7$ at $T = 20$°C, Bjerrum length $L_B = 1.55$ nm), and subjected to a broad range of added LiCl concentrations. Different from aqueous suspensions, this well-characterized system is not plagued by uncontrolled $CO_2$ contamination and self-dissociation of water molecules. Therefore, systems with very low salinities can be prepared. For our silica in DMF system, we have obtained a large body of static and short-time dynamic X-ray scattering data, for systems in the fluid-phase regime [10]. The small-angle X-ray scattering (SAXS) measurements were performed at the European Synchrotron Radiation Facility (ESRF) in Grenoble using synchrotron radiation at Troika III part of the ID 10A beamline in cooperation with the co-authors of Ref. [10]. The experimental details concerning the beamline and sample preparation are given in Ref. [10].

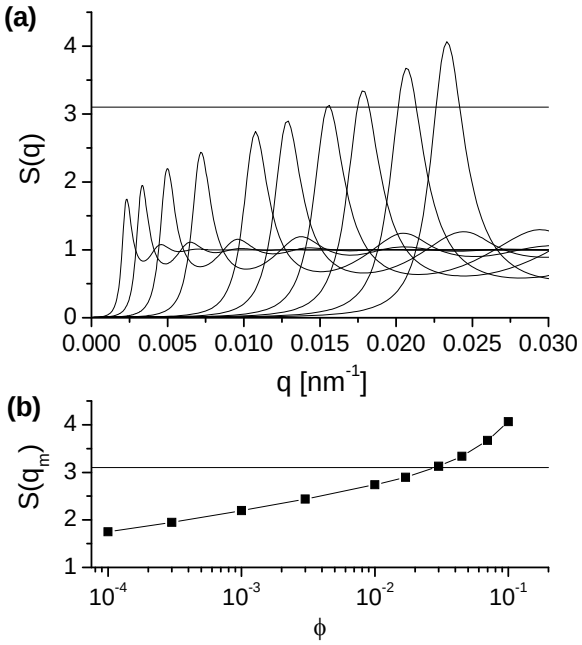


Fig. 1(a): RY-calculated static structure factor, $S(q)$, for salt-free suspensions at different volume fractions $\phi$ = 0.0001, 0.0003, 0.001, 0.003,0.01,0.017,0.03,0.045, 0.07, 0.1 (from left to right), and constant low-charge value Z = 300. (b) The principal peak height, $S(q_m)$, as a function of $\phi$. The horizontal lines mark the HV value, $S(q_m)$ = 3.1, used throughout this paper as indicator for the onset of freezing.

Different from Fig. 1, at very high effective charge values like the one considered in Fig. 2, $S(q_m)$ becomes a highly non-monotonic function in $\phi$. For very small concentrations, the peak height increases initially, traversing the freezing line at $\phi \approx 5\times10^{-8}$, subsequently passing through a high maximum (not resolved on the scale of Fig. 2b) which is located in the non-fluid volume fraction regime. When $\phi$ is further increased, a reentrant fluid phase is found according to the HV rule, in a concentration window of $0.0045 < \phi < 0.11$. For $\phi > 0.11$, the system freezes again.

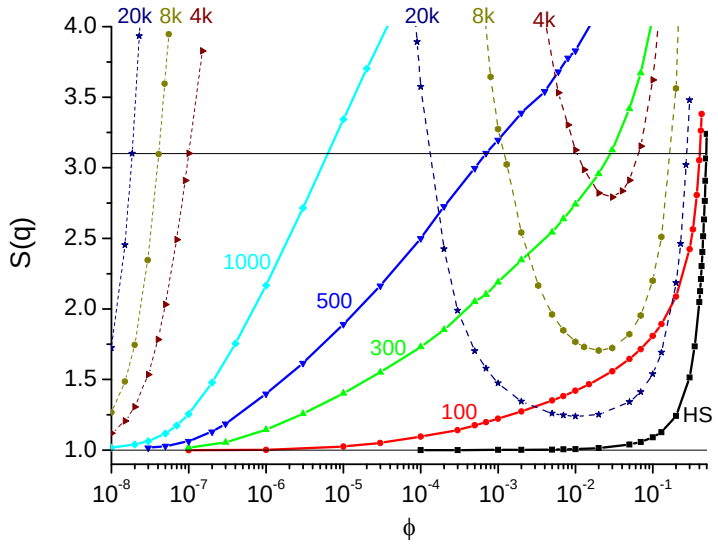


Fig. 3: RY static structure factor peak height, $S(q_m)$, as a function of ϕ, for values of $Z$ as indicated (1k = 1000), and constant $C_s$ = 0.001 μM. Solid lines are for $Z$ values in the small-charge region $Z$ = 0 – 1000. The dashed lines are the high-charge region results for $Z$ = 4000 – 20000.

Similar calculations of $S(q_m)$ have been performed also for several values of added salt concentration $C_s$. A summary of these results is shown in Fig. 4. In Fig. 4a, results for $S(q_m)$ are presented using a constant charge number of $Z$ = 500, representative of the "low charge" behavior (monotonic increase in $S(q_m)$), for six values of added salt concentration (0.001 μM to 1000 μM in decade steps). The line obtained for the largest $C_s$ is almost identical to the one describing a neutral hard-sphere system, whose $S(q_m)$ is also shown in the figure. In Fig. 4b, we demonstrate how the addition of salt affects the behavior of a system at $Z$ = 4000 e, which is a representative high-charge value for low-salt systems. The non-fluid phase region for intermediate values of ϕ , which is very broad for small $C_s$, narrows with increasing salt concentration and disappears for 0.5 μM < $C_s$ < 1 μM, although the non-monotonic behavior of $S(q_m)$ as a function of ϕ is still visible for $C_s$ ≈ 1 μM. Contrary to the low-charge case, a concentration of 1 mM added salt is not yet sufficient to reach the hard-sphere behavior.

and high-charge regions. In the low-charge (high-charge) region, $S(q_m)$ increases (decreases) with increasing $Z$. The width of both regions grows with increasing salinity. At a sufficiently large salinity, of value depending on the particle concentration, the two disjoint fluid-state regions merge into a single one, describing systems that do not freeze into a solid for any value of the effective charge (at this particular volume fraction). For a proper description of this merging, it is crucial to use an accurate integral equation method such as the RY scheme. Using a less accurate scheme such as the regularly applied analytic rescaled mean spherical approximation (RMSA), or the numerical hypernetted chain approximation (HNC), which both underestimate the particle ordering to some extent, could result in the prediction of the absence of a freezing transition for systems where freezing actually takes place. Moreover, precise integral equation methods such as the RY scheme, or the MPB-RMSA scheme [18], are necessary to obtain accurate values for the effective charge.

For the systems regarded in Fig. 5a, the maximum of $S(q_m)$ is located in between $Z$ = 1000 – 2000, with its position shifting to larger charge values for larger salt concentrations. Compare this to Fig. 3, where zero-salt systems are considered for fixed values of $Z$, and where $S(q_m)$ traverses a maximum as a function of $\phi$, when the surface-counterion contribution to $\kappa_{ci}^2 \propto \phi$ becomes sufficiently strong to overcompensate the ordering effect caused by the increasing particle concentration. When $\phi$ in Fig. 3 is further increased for a large-$Z$ system, $S(q_m)$ passes through a minimum observed at $\phi \sim 0.01 - 0.1$. The upswing of $S(q_m)$ at the largest considered $\phi$ values located to the right of this minimum, is due to the proximity of next-neighbor particles which are subject to a sharply rising pair energy.

[18]). The peak values $g_f(r_m)$ for the entire range of the system parameters will be thoroughly discussed in a related paper (labeled II).

The $Z$-dependence of $u(\langle r\rangle)$ and $u(r_m)$, for a constant $\phi$ and $C_s$ varying from $10^{-9}$ M to 20 μM, is analyzed in Fig. 5c. Even though $r_m$ is very close to $\langle r\rangle$ in low-salinity systems, the pair interaction energy changes so rapidly with distance that a slightly larger $r_m$ results in a distinctly lower value of the pair energy, and in the maximum of $u(r_m)$ shifted to a smaller value of $Z$. The maximum of $S(q_m)$ as a function $Z$ in Fig. 5a, is reflected by a corresponding maximum of $u(r_m)$ which is located, however, at a smaller value of $Z$. The maximum reflects the counterplay of the electric coupling strength, $\beta u(\sigma^+)$, and the counterion screening. The latter dominates for large $Z$ values. The vertical line pairs in Fig. 5c indicate the low-charge and high-charge values where freezing takes place. A fluid phase is found only outside these charge interval boundaries (bounded by the vertical lines). The pair energy at freezing is distinctly different for the low-charge and high-charge values. This points to the impossibility of formulating a freezing criterion in terms of $u(r_m)$ alone. The same degree of fluid ordering as quantified by $S(q_m)$ can be obtained for two distinctly different pair interaction energies. The behavior of $g_f(r_m)$ and $\beta u(r_x)$ at freezing will be discussed in detail in a related forthcoming paper (labeled II).

At this point, one should consider the physical relevance of the high-charge solutions for $S(q)$ and $g(r)$. Whether a high-charge solution is physically relevant depends on the system under consideration. There are limits to the maximal value the effective charge can attain in charge-stabilized suspensions set by the quasi-condensation of counterions (charge-renormalization effect), and by chemical charge regulation when weakly acid surface groups are present. As noted in the Introduction, estimates of the effective particle charge can be obtained from approximate Poisson-Boltzmann calculations with radial symmetry [33,35-36] and generalizations to multivalent microions [37]. The smallest values for the saturated

To avoid the latter problem, in our experiments we use DMF as the suspending solvent. The effective particle charge $Z$ is determined by the RY fit to the experimental structure factor peak height. The effective charge depends on $C_s$ and $\phi$ typically in an involved way through a general $Z = Z(L_B Z/a, \kappa a, \phi)$ dependence. For this reason, the iso-$Z$ freezing lines we are going to discuss in the following do not directly correspond to an actual experimental system. However, an experimental freezing line characterizing a concentration series can be easily constructed from a family of iso-charge freezing lines.

In Fig. 6, we show the $C_s$ - $\phi$ phase diagram with a family of iso-$Z$ freezing lines obtained from the RY scheme in combination with the HV freezing rule. The freezing lines for low-charge values (solid curves) increase monotonically in $\phi$, indicating that systems of larger salinity solidify at larger concentrations. With increasing Z in the low-charge region, the freezing lines move upwards, most strongly so at very small volume fractions. Accordingly, the area of the fluid-phase region extending into the upper left part of the phase diagram becomes smaller.

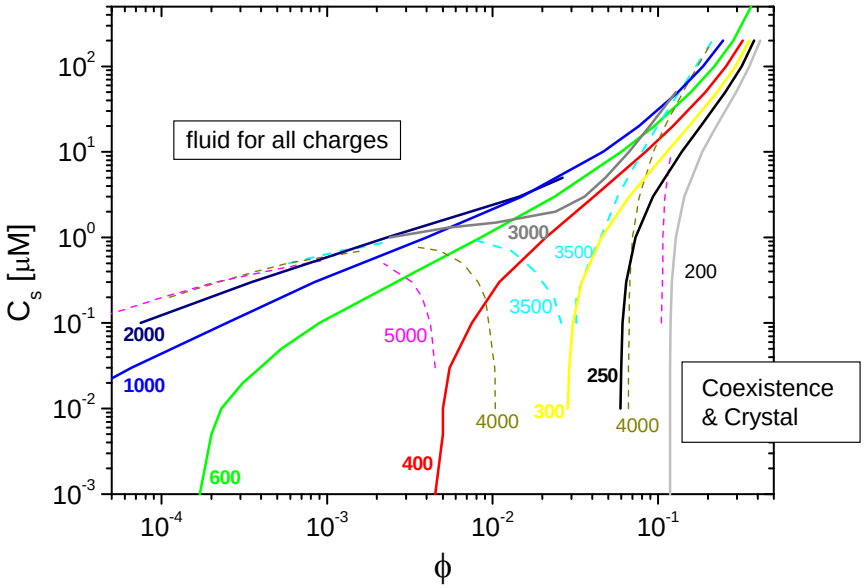


Fig. 6: $C_s$ - $\phi$ phase diagram for a charge series of iso-charge freezing lines, predicted using the RY scheme with $S_f(q_m) = 3.1$. Solid lines: low-charge freezing lines for charge values as indicated. Dashed lines: high-charge freezing lines.

From the experimental point of view, another convenient way to present the phase diagram of a Yukawa-like colloidal system is to use iso-ϕ freezing lines in the ($Z - C_S$) and iso-$C_S$ freezing lines in the ($Z$ - ϕ) coordinates. The ($Z$ – ϕ) phase diagram is presented in Fig. 7. In this figure freezing lines for different constant $C_S$ are shown which define values of $Z$ and ϕ at freezing for a Yukawa system.

Here, one clearly sees that at high ϕ all iso-$C_s$ freezing lines both for the low- and high-charge branches collapse on the corresponding lines of the salt-free system (two black lines), since for large ϕ the electric screening is dominated by the counter-ions. In Fig. 7, the low- and high-charge branches are easily distinguished. They merge continuously with each other with infinite slope at points where the system freezes at the lowest ϕ for a given $C_S$. Close to these points, the low- and high-charge values are similar and can be quite large, up to $10^5$. In agreement with the results in Figs. 3 and 4, for $C_s$ < 1 μM an iso-$Z$ horizontal line in Fig. 7 can intersect an iso-$C_S$ freezing line at only one ϕ value on the low-charge branch side. Additionally, there will be two phase transition points on the high-charge branch side, provided the added salt concentration $C_S$ is low enough, so that the iso-$C_s$ freezing line has a minimum at the intermediate concentration range of $0.01 < \phi < 0.1$. For low salt concentrations, three freezing transitions on the high-charge branch are also possible at $Z$ = const. For salt concentrations higher than about 1 μM, for the iso-$Z$ line there is one freezing transition point either on the low- or high-charge branch side.

defines the largest salt concentration, at the considered ϕ, for which the system can freeze. At higher salt concentrations the system remains fluid.

Recall from Figs. 3 and 4 that for low-charge systems, the iso-charge $S(q_m)$ vs. ϕ curve crosses the horizontal HV freezing line only at a single ϕ value, while for certain higher charge systems, three ϕ values are predicted where freezing can take place. In the iso-ϕ freezing line representation in Fig. 8, this corresponds to the feature that for lower charges (lower than about 3500), there is only a single constant-ϕ freezing line going through a point of given $C_S$-$Z$ coordinates, while in the higher charge region (above the dashed line in Fig. 8) there exist $C_s$ – $Z$ points corresponding to three different ϕ values. Thus, for an iso-$Z$ system at sufficiently large $Z$, a reentrant solid – fluid transition can be traversed when ϕ is increased.

Both the low- and high-charge branch effective charges in Figs. 7 and 8 at freezing increase strongly with decreasing colloid concentration. For very low ϕ ≈ $10^{-6}$ – $10^{-7}$ the values of both the low- and high charge values required for freezing are of the order of $10^5$e. However, it is questionable whether such large effective charge values can be attained in an experimentally realized system.

**D. Universal freezing line in the $\tilde{T}$ – λ phase space**

So far, we have discussed freezing line diagrams in terms of experimentally controllable parameters such as $C_s$ and ϕ. As noted in the Introduction, Yukawa-sphere systems, including the OCM-type colloid systems as a special case, where the physical hard core plays no role, are fully characterized in their equilibrium phase behavior by two dimensionless parameters, namely the reduced screening parameter, $\lambda = \kappa \langle r \rangle$, and the reduced temperature $\tilde{T} = k_B T / u\left(\langle r \rangle\right)$. The latter parameter is a measure of the thermal

value of $S_f(q_m)$ = 3.2 (open symbols). This serves to demonstrate that the universal freezing line is insensitive to smaller changes in selected HV peak value. The freezing line predicted by our RY-HV based data is in remarkably good overall agreement with the melting line predictions by Meijer and Frenkel (MF) [20], and Stevens and Robbins (SR) [22], and also with the more recent and more accurate MD simulation results for the melting line by Hamaguchi *et al.* [23].

In principle, one needs to distinguish the melting line from the freezing line, with the latter located somewhat above the former [25-26,40]. However, the difference between the two lines is quite small for smaller values of λ (small miscibility gap). This is illustrated in Figs. 9a and 9b, showing both the melting and freezing lines predictions of Stevens and Robbins [22]. In the one-component plasma limit of zero electric screening, for which $\tilde{T}(\lambda = 0)$ = $9.383\times10^{-3}$, the density difference between coexisting bcc and fluid phases becomes exactly zero, i.e., there is an isochoric transition [23]. We emphasize here that our RY-HV based results cover a large range of λ values, extending well beyond that explored earlier by Meijer and Frenkel [20], Stevens and Robbins [22], and Hamaguchi *et al*. [23].

Fig. 9b magnifies the lower-λ part of the phase diagram, which includes the bcc phase region. It displays the original melting line prediction by Robbins, Kremer and Grest (RKG) [16], in comparison to the more recent MD simulation results by Hamaguchi *et al*. [23]. According to Hamaguchi *et al*., the triple point of three-phase bcc-fcc-fluid coexistence is located at $\left(\tilde{T}_t, \lambda_t\right)$ = (0.2856, 6.90), i.e., at a screening value λ substantially larger than that predicted by RKG. According to Fig. 9b, the RKG melting line overestimates the melting temperature and thus the crystal stability. In the figure, we show additionally the state point of the 5 μM system of our silica in DMF H series (solid green points to the right) which will be addressed further down. This state point is located inside the bcc pocket region predicted by Hamaguchi *et al.*, but outside the RGK predicted bcc region. Only the bcc phase space pocket

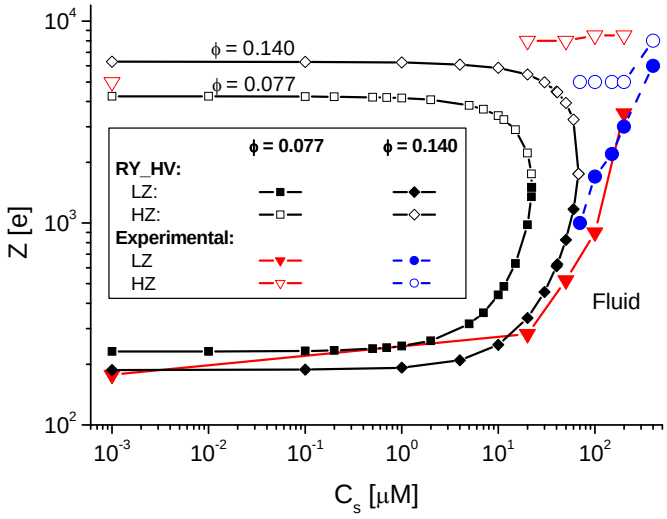


Fig. 11: Squares (diamonds) connected by straight line segments: RY-HV freezing line in the $Z$ -$C_s$ phase diagram for ϕ = 0.077 (ϕ = 0.140), obtained using $S_f(q_m)$ = 3.1. Solid and open symbols represent low- and high-charge freezing values of $Z$, respectively. Solid (open) red triangles: values of $Z(C_s)$ obtained from a RY-fit to the experimental $S(q)$ for the systems of series H (ϕ = 0.077) in [10] using the low- (high-) charge branch solution. Solid (open) blue circles: values of $Z(C_s)$ obtained from a RY-fit to the experimental $S(q)$ for the systems of series K (ϕ = 0.14) in [10] using the low- (high-) charge branch solution.

Consider in Fig. 11 first the lower-concentrated system at ϕ = 0.077. The lower (upper) part of the freezing line for the low-charge (high-charge) branch systems is determined by the RY-HV scheme using $S_f(q_m)$ = 3.1 (solid and open squares). According to the RY-HV rule, a homogeneous fluid phase exists only outside the region bounded by the two freezing line parts. For $C_s$ > 20 μM, no solid phase is predicted for any value of the effective charge.

In comparing the interconnected low- and high-charge freezing lines for ϕ = 0.14 (open and solid diamonds – series K) with those for ϕ = 0.077 (open and solid squares – series H), one notices from Fig. 11 that for the more concentrated K series systems the RY-HV predicted freezing values for $Z$ are located at lower (larger) values on the low-charge (high-charge) branch of the freezing line. Thus, the crystalline region of the phase diagram is broader for the more concentrated $C_s$ series, where crystallization is predicted to be absent for

crystallization is induced, at a value of $C_s$ roughly in the region of 1 μM. With further increasing $C_s$ (and $Z$), the screening effect by the surface-released counterions becomes so strong that the crystalline system melts again.

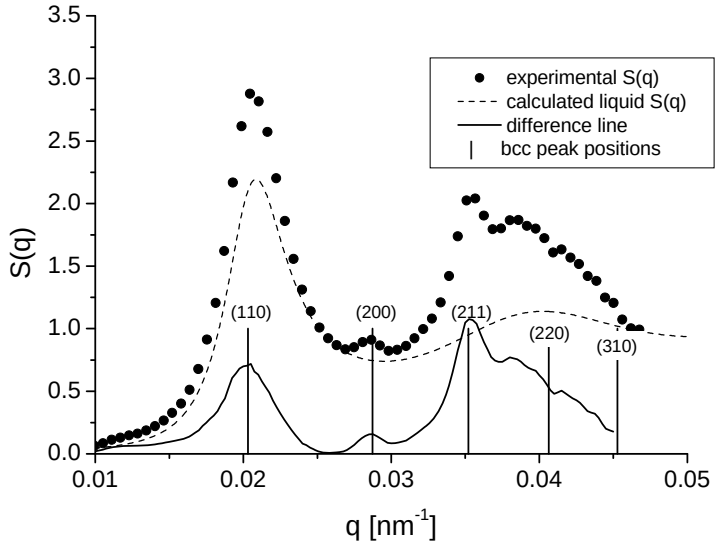


Fig. 12. Experimental SAXS structure factor (solid circles), RY calculated fluid-system $S(q)$ (dashed curve), and their difference values (solid curve), for the 5 μM salt content sample of series H. The vertical line segments indicate the wavenumber locations of the first few bcc lattice vectors (with Miller indices).

While our experimental study in [10] was focused on silica spheres in DMF systems located in the fluid phase regime, a few samples have shown clear evidence of crystalline order. An example of SAXS scattering data obtained for a $C_s$ = 5 μM sample of the H series, which was not discussed in [10], is given in Fig. 12. In this figure, symbols (solid circles) represent the experimental static structure factor data, and the dashed line corresponds to a fluid-like RY structure factor, calculated using parameters interpolated from the neighboring liquid points of series H [10]. The solid curve depicts the difference values between the experimental and RY-calculated structure factors.

From this difference curve, one can immediately recognize the presence of additional experimental peaks at $q \approx 0.020$, 0.029, 0.035 nm$^{-1}$, and a broad peak located in between $q$ = 0.037 nm$^{-1}$ and 0.045 nm$^{-1}$. The positions of these peaks can be nicely interpreted as the Bragg

branches (denoted by LZ and HZ, respectively) are clearly different. Regarding the H-series systems, the LZ-trajectory starts at low λ (salt-free case) in the fluid phase. Subsequently, at λ ≈ 5 ($C_S \approx 5$ μM), it enters the bcc crystal phase just to quickly return back into the fluid phase at slightly larger λ. Thus, a reentrant fluid – solid – fluid transition is experimentally observed indeed. The bcc structure of the crystal at λ ≈ 5 is corroborated by the SAXS Bragg peaks positions in Fig. 12, characteristic of a bcc crystal.

In Fig. 13, no reentrant behavior is observed in contrast to the HZ trajectory of the H-series (open red circles), which tends towards the fcc phase with decreasing λ (decreasing salt concentration). It is interesting to note that the lowest data point of this HZ trajectory corresponds to the salt-free sample represented in Fig. 11 by the open triangle at $C_S$ = $10^{-3}$ μM.

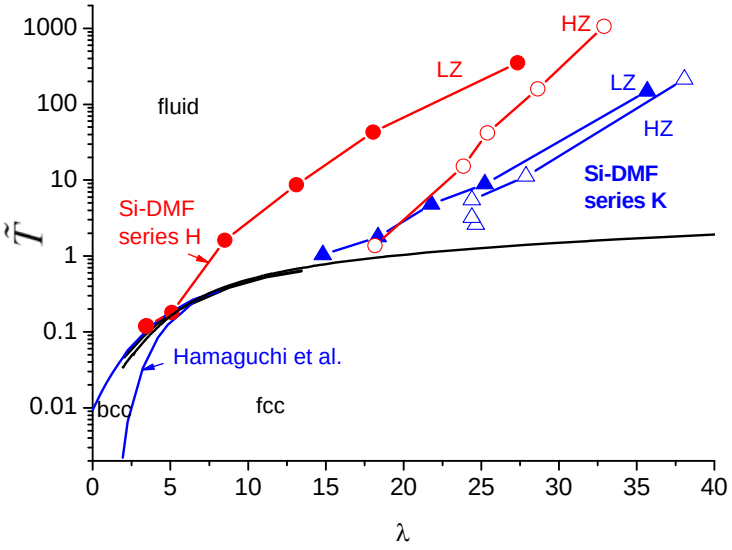


Figure 13. System trajectories of the H (red symbols) and K series (blue symbols) in the universal $\tilde{T}$ - λ phase diagram obtained by Hamaguchi *et al*. [23]. The black freezing line extending beyond the one of Hamaguchi *et al.* is composed of the freezing points presented in Figs. 6-8. "LZ" and "HZ" denote the low- and high-charge branch solutions, respectively.

The low- and high-charge trajectories of the experimental K series are qualitatively similar. Both trajectories approach the fcc crystal with decreasing λ (decreasing salt), however showing no reentrant transition. The LZ trajectory of series K starts very close to the

fcc solid (according to the RY-HV scheme) can be also observed for high salinities. In contrast, in high-charge branch systems where values $\lambda > 6.9$ are always found, freezing takes place only into an fcc solid. An additional criterion which can be used to identify the actual, experimentally occurring effective charge, provided the low-charge and high-charge values are largely different, are charge condensation/regulation considerations which give upper bounds to the experimentally realizable effective charge.

The universal $\tilde{T}$ - $\lambda$ freezing line traced out by our RY-HV results for $S(q_m) = 3.1$, is in good agreement with earlier simulation-based freezing and melting line predictions by various groups [16, 19-20, 22-23], thereby extending this line to a largely extended range of $\lambda$ values. We have checked that the universal freezing line is quite insensitive to small changes in the HV freezing value. Here, we re-emphasize that only systems with hard-core interactions masked by the electric repulsion have been considered, representative for most charge-stabilized systems.

The RY-HV based two-parametric space freezing lines have been used to analyze the system trajectories of two silica in DMF systems, one at $\phi \approx 0.077$ (series H) and the other at $\phi \approx 0.14$ (series K). Both systems were studied using SAXS as functions of added monovalent salt. We have shown experimentally, and in accord with the phase diagram calculations by Hamaguchi *et al.* [23] and our RY-HV based $Z - C_s$ phase diagram in Fig. 11, that a re-entrant fluid-solid-fluid transition takes place for the series H systems at constant colloid concentration, when the salt concentration is increased.

In the work by Royall et al. [6], a similar reentrant fluid – bcc - fluid transition has been observed experimentally for charged PMMA spheres in a solvent mixture as the volume fraction was increased. The unusual part in this sequence is the reentrant melting at a larger $\phi$. Royall et al. explain this sequence essentially by the strong $\phi$ dependence of the effective colloid charge which, in the considered concentration range, decreases with an increasing $\phi$.

Finally, we note that the behavior and the physical interpretation of the colloid-colloid pair energy in Yukawa sphere systems in relation to the pair structure and the $\tilde{T}$ - $\lambda$ freezing line will be discussed in the forthcoming paper II.

**Acknowledgments**

G.N. acknowledges support by the Deutsche Forschungsgemeinschaft (SFB-TR6, project B2) and helpful discussions with M. Heinen and A.J. Banchio. Partial support by the 'SoftComp' Network of Excellence (Grant No. S080118) is gratefully acknowledged. J.G. acknowledges support by the Human Capital Operating Program, Project 4.1.1 for the Faculty of Physics, Adam Mickiewicz University Poznan, Poland. The experimental data in Fig. 12 were obtained by SAXS experiments at ESRF reported in Ref. [10], in cooperation with J. Buitenhuis, P. Holmqvist, P. Lettinga, and G. Meier (Reseach Centre Jülich, Germany). We thank them for their permission to show these data in the present paper.

[14] F. Roosen-Runge, M. Hennig, F. Zhang, R.M.J. Jacobs, M. Sztucki, H. Schober, T. Seydel, and F. Schreiber, *PNAS* **108**, 11815 (2011).

[15] AF. Zhang, M.W.A. Skoda, R. M. J. Jacobs, R.A. Martin, C. M. Martin, and F. Schreiber, *J. Phys. Chem. B* **111**, 251 (2007).

[16] O. Robbins, K Kremer, and G. S. Grest, *J. Chem. Phys.* **88**, 3286 (1988).

[17] A.-P. Hynninen and M. Dijkstra, *J. Phys.: Condens. Matter* **15**, S3557 (2003).

[18] M. Heinen, P. Holmqvist, A. J. Banchio, and G. Nägele, *J. Chem. Phys.* **134**, 044532 & 129901 (2011).

[19] K. Kremer, M.O. Robbins, and G.S. Grest, *Phys. Rev. Lett.* 57, 2694 (1986).

[20] E.J. Meijer and D. Frenkel, *J. Chem. Phys.* **94**, 2269 (1991).

[21] E.J. Meijer and F. El Azahar, *J. Chem. Phys.* **106**, 4678 (1997).

[22] M.J. Stevens and M.O. Robbins, *J. Chem Phys.* 98, 2319 (1993).

[23] S. Hamaguchi, R.T. Farouki, and D.H. E. Dubin, *Phys. Rev. E* **56**, 4671 (1997).

[24] O.S. Vaulina and S.A. Khrapak, *J. Exp. Theor. Phys.* **92**, 228 (2001).

[25] D.C. Wang and A.P. Gast, *J. Phys.: Condens. Matter* **11**, 10133 (1999).

[26] D.C. Wang and A.P. Gast, *J. Chem. Phys.* **112**, 2826 (2000).

[27] A.-P. Hynninen and M. Dijkstra, *Phys. Rev. E* **68**, 021407 (2003).

[28] P. N. Pusey, in: *Liquids, Freezing and Glass Transition*, Les Houches Sessions 1989, eds. J.-P. Hansen, D. Levesque, and J. Zinn-Justin (North-Holland, Amsterdam, 1991) pp. 763-942.

[29] T.V. Ramakrishnan and M. Yussouf, *Phys. Rev. B* **19**, 326 (1979).

[30] T.V. Ramakrishnan, *Phys. Rev. Lett.* **48**, 541 (1982).

[31] J.-P. Hansen and L. Verlet, *Phys. Rev.* **184**, 151 (1969).

[32] J. Gapinski, A. Patkowski, G. Nägele, *J. Chem. Phys.* **132**, 054510 (2010).

**Figure captions**

Fig. 1(a): RY-calculated static structure factor, $S(q)$, for salt-free suspensions at different volume fractions $\phi$ = 0.0001, 0.0003, 0.001, 0.003,0.01,0.017,0.03,0.045, 0.07, 0.1 (from left to right), and constant low-charge value Z = 300. (b) The principal peak height, $S(q_m)$, as a function of $\phi$. The horizontal lines mark the HV value, $S(q_m)$ = 3.1, used throughout this paper as indicator for the onset of freezing.

Fig.2(a): RY static structure factor for "salt-free" suspension at volume fractions $\phi$ = 1, 2, 3, 4, 5, 6, 7, $8\times10^{-8}$ (left group) and $\phi$ = 0.002, 0.003, 0.0045, 0.007, 0.01, 0.02, 0.03, 0.05, 0.07, 0.1, 0.13, 0.15 (right group), using a large effective charge value of $Z$ = 5000. (b) Principal peak height $S(q_m)$ as a function of $\phi$ plotted on a linear-log scale. The horizontal lines mark the HV value, $S(q_m)$ = 3.1, used throughout this paper as indicator for the onset of freezing.

Fig. 3: RY static structure factor peak height, $S(q_m)$, as a function of $\phi$, for values of $Z$ as indicated (1k = 1000), and constant $C_s$ = 0.001 μM. Solid lines are for $Z$ values in the small-charge region $Z$ = 0 – 1000. The dashed lines are the high-charge region results for $Z$ = 4000 – 20000.

Fig. 4: Added salt concentration dependence of $S(q_m)$, (a) for a low-charge value of $Z$ = 500, and (b) for a high-charge value of $Z$ = 4000. The numbers at the solid curves are the salt concentrations, $C_s$, in μM (1k = 1000). The lowest curves in (a) and (b), labeled by HS, represent the neutral hard-sphere results. Horizontal lines: $S(q_m)$ = 3.1.

Fig. 5. $Z$-dependence of (a) the static structure factor maximum $S(q_m)$, (b) the radial distribution function maximum $g(r_m)$, and (c) the pair interaction energy at $r_x = \langle r \rangle$ (solid symbols) and at $r_x = r_m$, (open symbols) calculated using the RY scheme for $\phi$ = 0.077,

Fig. 10: $\tilde{T} - \lambda$ phase-space trajectory of the high-charge, zero-salinity concentration series system of Fig. 2b (blue solid line). The arrows on the blue line indicate the direction of increasing $\phi$. The trajectory starts in the fluid phase at an extremely low concentration $\phi \sim 10^{-8}$, crossing next the bcc and then the fcc crystal phase at around $\phi = 6.82\times10^{-8}$, returning to the fluid phase at $\phi = 4.39\times10^{-3}$, and finally crossing into the fcc phase at $\phi \sim 0.10$. Inset: $\phi$ dependence of $\lambda$ and $\tilde{T}$ along the trajectory.

Fig. 11: Squares (diamonds) connected by straight line segments: RY-HV freezing line in the $Z$ -$C_s$ phase diagram for $\phi = 0.077$ ($\phi = 0.140$), obtained using $S_f(q_m) = 3.1$. Solid and open symbols represent low- and high-charge freezing values of $Z$, respectively. Solid (open) red triangles: values of $Z(C_s)$ obtained from a RY-fit to the experimental $S(q)$ for the systems of series H ($\phi = 0.077$) in [10] using the low- (high-) charge branch solution. Solid (open) blue circles: values of $Z(C_s)$ obtained from a RY-fit to the experimental $S(q)$ for the systems of series K ($\phi = 0.14$) in [10] using the low- (high-) charge branch solution.

Fig. 12. Experimental SAXS structure factor (solid circles), RY calculated fluid-system $S(q)$ (dashed curve), and their difference values (solid curve), for the 5 μM salt content sample of series H. The vertical line segments indicate the wavenumber locations of the first few bcc lattice vectors (with Miller indices).

Figure 13. System trajectories of the H (red symbols) and K series (blue symbols) in the universal $\tilde{T}$ - $\lambda$ phase diagram obtained by Hamaguchi *et al*. [23]. The black freezing line extending beyond the one of Hamaguchi *et al.* is composed of the freezing points presented in Figs. 6-8. “LZ” and “HZ” denote the low- and high-charge branch solutions, respectively.